Experimental Approach to Physicochemical Hydrogen Processes on Cosmic Ice Dust

Naoki Watanabe* and Masashi Tsuge

Institute of Low Temperature Science, Hokkaido University, Sapporo 060-0819, Japan

Abstract

Hydrogen is the most abundant element in the universe, and thus atomic and molecular hydrogen play important roles in chemical evolution in space. In particular, the physicochemical processes of hydrogen on cosmic dust, such as the diffusion of H atoms and nuclear spin conversion of H_2 molecules at low temperatures, are recognized to significantly influence the subsequent chemical evolution. However, it is not easy to track the hydrogen on the surface by conventional experiments. We have recently succeeded in applying a combination of photostimulated desorption and resonance-enhanced multiphoton ionization methods to detect hydrogen on cosmic dust analogues. In this paper, we present a brief review of our recent experiments for elucidating the behavior of hydrogen on water ice, pure solid carbon monoxide, and diamond-like carbon as cosmic dust analogue surfaces.

1. Introduction

The birthplace of stars and planets, namely, the interstellar cloud,[1-3] which consists of gaseous species and cosmic silicate dust, can be considered as the starting point of chemical evolution in space, where most of the relatively light elements, such as hydrogen, carbon, oxygen, and nitrogen, first exist as atoms. When an interstellar cloud gravitationally shrinks, it becomes a cold dense region, a so-called molecular cloud (MC). The number densities of gas in MCs range from 10^3 to 10^6 cm^{-3}.[4] The temperature of an MC can be down to 10 K because the large amounts of cosmic dust shield the inside of the MC from external radiation fields. In the MCs, the complexity of the molecules explosively increases despite the low temperatures. To date, more than 150 species including organic molecules have been assigned[5] in both the gas phase and ice solids,[6, 7] namely, ice mantles, which cover the silicate dust most abundantly with H_2O molecules. Hydrogen plays an important role in the formation of such molecules.[8] The motivation of our research is to understand how and when these molecules are formed from atoms and simple molecules.

Among the astronomically observed molecules, abundant species such as H_2 and H_2O and primordial organic molecules such as formaldehyde (H_2CO) and methanol (CH_3OH) require synthesis by surface reactions on the dust to reach their observed abundances.[8-10] For example, the direct formation of H_2 in the gas phase by the radiative association of two H atoms in the ground state is forbidden. When one of the H atoms is in the electronic excited state, though, the radiative association becomes allowed. However, the collision rate of two H atoms in the gas phase is approximately once a year, and thus reactions including the electronic excited state are not realistic in MCs. In contrast, when two H atoms encounter each other on the surface of dust, the heat of the

association reaction can be dissipated by the surface without emitting a photon. This third body effect of the surface is one of the advantages of surface reactions. Therefore, it has been widely accepted that H_2 molecules are created by H-H recombination reactions on dust, even without experimental proof.[11] The recombination reaction itself would proceed immediately even at approximately 10 K once the atoms encounter each other, because radical-radical association reactions tend to be barrierless. Therefore, the H_2 formation rate would be limited by the surface diffusion of H atoms. To confirm the idea of the H_2 formation on dust, quantitative experiments of the H atom diffusion on the surface of a dust analogue, mainly water ice, are desirable.

H_2O, H_2CO, and CH_3OH molecules have been found abundantly as solids in the ice mantles that cover the cosmic dust.[6, 7, 12] The observed abundances of these molecules cannot be explained by the gas-phase synthesis and subsequent freeze-out on the dust, and thus surface reactions are necessary. The surface reactions on a silicate dust start with H_2O formation as the main component of the ice mantle. Once H_2O forms the first layer of ice on a silicate dust, subsequent reactions occur on the water ice. It has been demonstrated that H_2O, H_2CO, and CH_3OH are efficiently produced on water ice even at approximately 10 K by successive reactions of H atoms with O_2 and CO: $O_2 \xrightarrow{H} HO_2 \xrightarrow{H} H_2O_2 \xrightarrow{H} OH + H_2O$ [13-15] and $CO \xrightarrow{H} HCO \xrightarrow{H} H_2CO \xrightarrow{H} CH_3O \xrightarrow{H} CH_3OH$.[13, 16-19] In the series of reactions, the last step of the O_2 hydrogenation and the first and third steps of the CO hydrogenation proceed via tunneling (tunneling hydrogenation) because these reactions have significant activation barriers corresponding to 2500–3500 K[20-23] and therefore cannot occur thermally at approximately 10 K. The tunneling hydrogenation is one of the important features that

enhances the molecular formation on cryogenic dust surfaces, where the wave nature of hydrogen becomes prominent.[24] In the typical experiments, reactants on ice were exposed to H atoms with significant fluxes up to 10^{14} cm^{-2} s^{-1}, where the H atoms easily reach the reactants on the surface. In contrast, on a realistic dust surface, adatoms need to migrate for a long distance to encounter their reaction partners, because the accretion rate of the atoms is approximately once a day and thus the surface coverage of the atoms should be very low. In such a circumstance, reaction rates are often limited by diffusion. Therefore, to evaluate surface reactions quantitatively, the surface diffusion of H atoms should be clarified.

As described above, the surface diffusion of H atoms at low temperatures is a key to quantitatively understanding the molecular formation on cosmic dust. However, it is not easy to monitor the H atoms experimentally for the following reasons. The H atoms desorb at very low temperatures, typically below 20 K, because the interactions between the H atoms and the surfaces of water ice and other dust materials are very weak (physisorption). Therefore, the diffusion is very fast and sensitive to the temperature. Furthermore, the temperature window where the surface atoms can be monitored is narrow. Microscopic techniques such as STM, FEM, and AFM often used for monitoring adsorbates are not powerful for detecting H atoms in such conditions. In addition, pure water ice is not an electrical conductor. Although electron paramagnetic resonance (EPR) spectroscopy can follow the radical diffusion, it is not surface-sensitive. Instead, the surface diffusion of H atoms on ice has often been investigated by temperature-programmed desorption (TPD) experiments.[25] In the TPD experiments, H or deuterium (D) atoms are deposited at 10 K on water ice in the amorphous phase (amorphous solid water: ASW), because the ice mantles in MCs are found to consist mainly of ASW.[26] The

physical properties of ASW differ to some extent from those of crystalline ice especially in density and structure.[8] Generally, ASW has various defects, such as micropores and cracks, and irregular surface. The deposited adatoms recombine to form H_2, HD, or D_2 upon heating the ASW, and the produced molecules are thermally desorbed and detected by a quadrupole mass analyzer as a function of the surface temperature. The TPD spectra are typically analyzed with rate equations for recombination and desorption including the activation energies for the diffusion of atoms and molecules and for desorption as free parameters. However, multiparameter fittings often result in large uncertainties. Furthermore, the diffusion barriers cannot be represented by a single value but should have a wide distribution on the irregular surface of the ASW. The site-resolved experiments are necessary to solve this problem. Consequently, TPD and other macroscopic experimental methods are not suitable for determining surface diffusion barriers. In fact, TPD experiments sometimes provided contradictory results.[27, 28]

For better understanding chemical evolution, the hydrogen diffusion on cosmic dust materials needs to be elucidated by appropriate methods of experiment. Recently, using a combination of photostimulated desorption (PSD)[29] and resonance-enhanced multiphoton ionization (REMPI) methods, we were successful in monitoring hydrogen on ASW,[30, 31] polycrystalline ice (PCI),[30-32] pure solid CO,[33] and diamond-like carbon.[34] In the following sections, a summary of these experiments is provided after the description of the PSD-REMPI method. Additionally, as our new experimental findings relevant to the hydrogen diffusion, a proton-hole transfer that delivers a negative charge through ice is presented (Sect. 6).

Another astronomically important issue related to hydrogen is the ortho-to-para ratio (OPR) of H_2 molecules.[35-40] A hydrogen molecule consists of two protons, and thus

the total nuclear spin becomes 0 or 1, which are referred to as the para and ortho states, respectively. According to the Pauli exclusion principle, the ortho and para hydrogen can only take odd and even numbers for the rotational state, respectively. The energy difference between the lowest para (J = 0) and ortho (J = 1) states in the gas phase is approximately 14.7 meV, which corresponds to approximately 170 K. This energy is significant in MCs, and the heat capacity of H_2 gas thus depends on the OPR.[41] Therefore, the OPR of H_2 affects not only the chemistry but also the gas dynamics leading to star formation.[42] The radiative transition between these two states is forbidden. In the gas phase, spin-exchange reactions with either ionic or neutral hydrogen can alter the OPR of H_2.[43-46] It was often assumed without experimental evidence that the OPR of the H_2 formed on the cosmic dust surface has a statistical value of 3.[47, 48] Recently, we approached these issues experimentally, as described in Sect. 7.[30, 49]

2. PSD-REMPI method

The PSD-REMPI method does not measure the hydrogen adsorbates on the surface in situ but rather the amount of photodesorbed hydrogen adsorbates, whose intensity is proportional to the surface number density, as a snapshot. Fig. 1 shows a timing chart of the typical PSD-REMPI measurement for detecting the H atoms continuously deposited on ASW. The flux of H atoms was on the order of 10^{12} cm^{-2} s^{-1}. The PSD was caused by an unfocused weak laser radiation at 532 nm with energies less than 80 μJ pulse^{-1}. The REMPI laser was focused approximately 1–2 mm above the surface. The (2+1) REMPI spectra of the H atoms were obtained through two-photon absorption for the excitation to the intermediate 2*s* state and an additional one photon for ionization.[50] By changing the delay between the PSD and REMPI laser shots, the

translational energy distribution of the desorbed species can be obtained as the variation of the REMPI signal intensity. The mechanism of PSD is not clear because both the adsorbate and ice in the physisorption cases are transparent to photons at 532 nm. The translational energy distributions were independent from the PSD laser power and reproduced by the Maxwell-Boltzmann distributions at 30–50 K. [32] Therefore, the adsorbates may be mildly desorbed by phonon propagation from the metal substrate. Fig. 2(a) shows the PSD-REMPI spectra at the delays for the maximum intensities. As seen in Fig. 2(b), the REMPI spectral intensities increase linearly with the deposition time, ensuring that this method can monitor the amount of photodesorbed H atoms proportional to the surface number density.

3. Surface diffusion of H (D) atoms on ASW and PCI

3.1 ASW

To clarify the diffusion mechanism of atomic hydrogen, thermal or tunneling, we first measured the isotope effect on the surface diffusion of atomic hydrogen on ASW.[30, 32] The experimental procedure is shown in Fig. 3. The ASW surface was made on an aluminum substrate by the vapor deposition of up to 40 monolayers of H_2O (D_2O) through a capillary plate. The H (D) atoms were produced by the dissociation of H_2 (D_2) gas in microwave-induced plasma with a dissociation fraction of 70–80% and deposited through a cold aluminum pipe to reduce the translational energy to 100 K.[51] A given number of H (D) atoms were deposited on the surface of ASW at approximately 10 K, and after a given time period, t, the atoms were detected by the PSD-REMPI method. The number density of H (D) atoms on the surface, $n_{H,D}$, is expected to decrease by monoatomic desorption and/or H-H (D-D) recombination to form H_2 (D_2) molecules and thus can be

expressed by

$$\frac{dn_{\mathrm{x}}}{dt} = -k_{\mathrm{x-x}}n_{\mathrm{x}}^2 - k_{\mathrm{des\text{-}x}}n_{\mathrm{x}}, \qquad (1)$$

where "x" denotes H or D, $k_{\mathrm{x-x}}$ is the recombination rate constant, and $k_{\mathrm{des\text{-}x}}$ is the monoatomic desorption rate. When the monoatomic desorption is negligible at very low temperatures, the decrease rate is governed only by recombination. To evaluate the contribution of the recombination and monoatomic desorption of H atoms to the decrease rate, we measured the PSD-REMPI intensities of H_2 for continuous H atomic and H_2 molecular deposition on both a bare aluminum substrate and ASW at 8 K. The H atoms and H_2 molecules were deposited through the atomic source at the same H_2 gas flow rate with and without microwave operation, respectively. The H_2 molecules were selectively ionized by (2+1) REMPI through E, F^1 ($v' = 0, J' = J$) ← X^1 ($v = 0, J = 0$ or 1) transitions.[52] As shown in Fig. 4, the H_2 intensities behave differently for the aluminum and ASW surfaces.[32] For the aluminum surface, the H_2 intensities for H atom deposition are smaller than those for H_2 deposition, indicating that more than half of the deposited hydrogen is lost from the surface during H atom deposition, while a portion of the H_2 formed by H-H recombination and H_2 undissociated in the atomic source remain on the surface. In contrast, for the ASW surface, the H_2 intensities for the H atom deposition are almost equivalent to those for the H_2 deposition. This result clearly shows that most of deposited H atoms recombined and remained as H_2 on the surface without desorption by the heat of the association reaction. As a result, when a certain amount of H atom is deposited on ASW at 8 K, it decreases predominantly by recombination. That is, the second term on the right side in Eq. (1) can be ignored. Fig. 5 shows the decreases of H or D atoms on ASW at 8 K when the initial surface coverage, θ, of the atoms was approximately 2–7 × 10^{-2}. At such low coverages, the recombination rate should be limited by surface diffusion

because the recombination itself is a radical-radical barrierless reaction in the physisorption system. The isotope effect on the decrease rate was found to be small, indicating that the surface diffusion is dominated by thermal hopping rather than tunneling under this experimental condition. Solving Eq. (1) and deleting the monoatomic desorption term, the plots for 8 K in Fig. 5 can be well fitted by

$$\frac{I_{\mathrm{H}}}{I_0} = \frac{n_{\mathrm{H}}}{n_0} = \frac{1-b}{k_{\mathrm{x-x}} n_0 t + 1} + b, \qquad (2)$$

where I_{H} and I_0 are PSD-REMPI signal intensity of H atoms at time t and t = 0, respectively, and n_{H} and n_0 are the corresponding surface number density of H atoms. An asymptotic value, b, arises from the existence of H atoms that are long-lived even after 90 minutes. Although we cannot derive $k_{\mathrm{x-x}}$ and n_0 independently, their product, $k_{\mathrm{x-x}}n_0$, can be determined. For the thermal hopping, when the recombination is limited by diffusion, the following equation can be obtained:

$$k_{\mathrm{x-x}} = s\, v \exp\left(\frac{-E_{\mathrm{diff}}}{k_{\mathrm{B}} T}\right), \qquad (3)$$

where s, v, and E_{diff} are the unit area of the surface site, a frequency factor which is typically 10^{12}–10^{13} s^{-1}, and an activation barrier for diffusion, respectively. Because the coverage of the H (D) atom, θ, can be written as $\theta = sn_0$, Eq. (3) converts to

$$k_{\mathrm{x-x}} n_0 = \theta\, v \exp\left(\frac{-E_{\mathrm{diff}}}{k_{\mathrm{B}} T}\right). \qquad (4)$$

From Eq. (4) and fitting the plots in Fig. 5 with Eq. (2), we determined $E_{\mathrm{diff}} = 22 \pm 1$ and 23 ± 1 meV for H and D atoms, respectively. As expressed by the parameter b in Eq. (2), some H and D atoms did not encounter each other within 90 minutes at 8 K ($b \sim 0.2$ and 0.3 for H and D atoms, respectively: see Fig. 5). This indicates the existence of energetically deep potential sites on the ASW surface in which the H (D) atoms are trapped. We estimated the value of E_{diff} for a deep site to be more than approximately 30

meV, as shown by the dotted line in Fig. 5. The obtained distribution of E_{diff} covers those reported previously.[27, 28)]

3.2 PCI

When the surface number density of H and D atoms on the PCI surface is probed by the method described above, the intensities of both the H and D atoms rapidly decreased as shown in Fig. 5. This result implies that the H atoms under these conditions were much more rapidly consumed by recombination following fast diffusion compared with the situation for ASW at 8 K and it is difficult to track the surface number density of H atoms by the PSD-REMPI method after the deposition of a given amount of H atom. This may be partly ascribed to the fast tunneling diffusion and subsequent recombination. To evaluate the tunneling diffusion of H atoms on the PCI, we employed another methodology.[31)]

When H (D) atoms are continuously deposited on the PCI, the surface number density is determined by the balance between the supply from the atomic source and the loss due to recombination at low temperatures where the monoatomic desorption is negligible:

$$P_{ad} f_x = k_{x-x} n_x^2 , \qquad (5)$$

where P_{ad} and f_x are the adsorption coefficient and flux of H (D) atoms, respectively. According to molecular dynamics calculations, the difference in the adsorption coefficients of the H and D atoms is very small when the collisional temperature of the H and D atoms is approximately 100 K.[53)] Therefore, it is reasonable to assume an equivalent P_{ad} for H and D atoms under our experimental conditions. When the fluxes of H and D atoms are almost the same, the ratio of the surface number densities is simply expressed in terms of the H-H and D-D recombination rate constants as

$$\frac{n_{\mathrm{D}}}{n_{\mathrm{H}}} \approx \sqrt{\frac{k_{\mathrm{H-H}}}{k_{\mathrm{D-D}}}}. \qquad (6)$$

Considering that recombination is a radical-radical barrierless reaction and thus limited by the surface diffusion, we can derive the ratio of the diffusion coefficients from that of the number densities of H and D atoms by Eq. (6). Therefore, measurements of the number density ratios for H and D atoms can provide the isotope effect on the diffusion coefficient.

The surface of PCI consists of many small pieces of single crystalline ice.[54] We deduce that the H atoms diffuse via tunneling within a single crystalline surface where the adsorption sites have periodic-like shallow barriers for diffusion, while diffusion for a long distance over grain boundaries and steps is thermally limited. That is, when H atoms are distributed within a single crystal at higher coverages, they can diffuse rapidly via tunneling followed by recombination within a single crystal. On the other hand, when atoms are required to overcome grain boundaries and steps to encounter another atom at lower coverages, the recombination would be limited by the slower thermal hopping. To confirm this scenario, we performed an experiment where the coverage of H (D) adatoms was indirectly controlled by changing the atomic fluxes impinging. Fig. 6 shows the ratio of the H and D atom intensities obtained by the PSD-REMPI method in the steady state during the continuous deposition on PCI and ASW at various fluxes. Assuming that the activation barriers of thermal hopping are 22 and 23 meV for H and D atoms,[32] respectively, and that the frequency factor, ν, is inversely proportional to the mass in Eq. (3), $k_{\mathrm{H-H}}/k_{\mathrm{D-D}}$ becomes approximately 4.5 at 10 K, which corresponds to $n_{\mathrm{D}}/n_{\mathrm{H}} = 2.12$. Therefore, the signal ratio of $n_{\mathrm{D}}/n_{\mathrm{H}}$ in Fig. 6 at lower fluxes can be explained by thermal hopping. However, the $k_{\mathrm{H-H}}/k_{\mathrm{D-D}}$ ratios at approximately 100 for PCI certainly indicate a

significant isotope effect characteristic of tunneling diffusion.[55, 56] The atomic flux dependence of the k_{H-H}/k_{D-D} was seen even for the ASW surface and, as flux increases, the value approaches the asymptotic value ~16, which is larger than the value 4.5 expected for thermal hopping. Although these results indicate the coexistence of quantum tunneling and thermal diffusion, thermal hopping may still be the dominant mechanism controlling the surface diffusion of H and D atoms on the ASW surface because of poor energy-level matching in irregular potentials.[31, 57-59]

4. Surface diffusion of H (D) atoms on solid CO

Carbon monoxide (CO) is the second most abundant molecule, after H_2, in the gas phase of MCs and also exists in ice mantles of cosmic dust. It is known that the cosmic dust in some MCs is covered with solid CO.[7, 60, 61] To understand the molecular formation on such dust, the diffusion of H atoms on pure solid CO needs to be clarified. In contrast to the extensive studies on the diffusion of H atoms on ASW, little has been known about that on pure solid CO. One theoretical study reported the activation barrier of H-atom diffusion on crystalline CO (110) surface to be ~6–15 meV in the temperature range from 70 to 170 K.[18] However, the distribution of the adsorption potential depth on a realistic dust should be different from that of crystalline CO and, thus, an experimental determination of activation barriers of H-atom diffusion on solid CO is important. Using the method described in Sect. 3.1, we performed experiments to determine the mechanism of diffusion of H and D atoms on pure solid CO and to derive the activation energies of the diffusion process.[33]

About 30 monolayers of pure solid CO were vapor-deposited onto an aluminum substrate kept at 8 K. The H (D) atoms were deposited on pure solid CO at 8, 12, and 15

K with maximum atomic coverages, θ, of ~2.5 × 10^{-4}, 8.6 × 10^{-5}, and 7.7 × 10^{-5}, respectively. It was confirmed that the losses of adatoms by monoatomic desorption and reaction to produce HCO are negligible after the deposition; therefore, the attenuation of adatoms should be caused by the recombination reaction following surface diffusion. Fig. 7 shows the attenuation of H (D) atoms on solid CO; filled and open squares represent the measurements of H and D atoms, respectively, at a temperature of 8 K. Because no significant isotope effect was observed (see Fig. 7), the diffusion is limited by thermal hopping and, therefore, the data points should be fitted by Eq. (2). Using Eq. (4), the activation barriers for H atom surface diffusion are derived to be ~22, 30, and 37 meV for 8, 12, and 15 K, respectively. It should be noted that these are representative values based on the dominant diffusion rates at each temperature. At higher temperatures, the H atoms tend to be accommodated in deeper potential sites, suggesting that the diffusion of the H atoms is limited by the larger activation energies. Because the CO ice was vapor-deposited at approximately 10 K, the surface is considered rough and has various potential sites. There must be shallower potential sites that lead to lower activation barriers than the obtained ones.

5. Behavior of H (D) atoms on diamond-like carbon

A high H_2 formation rate has been inferred from the observation of regions where the temperature is too high for interstellar grains to be covered with icy mantles,[62, 63] indicating that the bare grain surface plays a role in producing H_2. Compared to H_2 formation processes on ASW and other astronomical ice analogues,[24] laboratory investigations of these processes on bare grain surface analogues are quite limited.[64, 65] According to infrared astronomy,[66] bare dust grains mainly consist of silicate or

carbonaceous materials, although the specific composition and morphology remain unclear. A diamond-like carbon (DLC),[67, 68] in which sp^3-hybridized C-C bonds dominate, can be a model surface compound, considering the ubiquity of nanodiamonds in the ISM.[69, 70] Recently, we successfully produced a hydrogen-free DLC surface by the laser ablation method and investigated the H (D) atom diffusion processes on it.[34]

We found that the H atoms on DLC cannot be detected by the PSD-REMPI method, in contrast to those demonstrated for ASW and CO surfaces.[30, 33] Instead, we decided to monitor the surface number density of H_2 upon H atom deposition to extract information on the H atom diffusion. Figs. 8(a) and 8(b) show the evolution of the surface H_2 number density on DLC upon H_2 and H atom deposition with the temperature of the DLC sample at 8 and 20 K, respectively. When the temperature of the DLC sample was 8 K, the H_2 number density upon H_2 deposition is approximately 1.5 times greater than that upon H atom deposition. This result indicates that, upon H atom deposition, a portion of the adsorbed H atoms remains unreacted, and the recombined and undissociated H_2 stays on the surface. This interpretation has been supported by temperature-programmed desorption (TPD) experiments, in which the TPD spectrum measured after H_2 deposition was nearly identical to one measured after H atom deposition (equivalent dose). The signal intensity ratio of 1.5 means that 50% of the adsorbed H atoms recombined to form H_2. The ratio of the H_2 signal (1.5 at 8 K) decreased as the temperature increased and reached almost unity at 20 K: see Fig. 8(b). This result indicates that, at 20 K, almost all the adsorbed H atoms readily recombine to form H_2. When similar experiments were performed with D_2 and D atoms, the signal intensity ratio stayed constant at approximately 2.0 in the temperature range 8–20 K (Figs. 8(c) and 8(d)). This constant ratio means that the fraction of D atoms that remain unreacted on the DLC surface is

constant (~70%) for this temperature range, in contrast to the high recombination efficiency of H atoms at 20 K. This large kinetic isotope effect on recombination (diffusion) indicates the occurrence of quantum tunneling diffusion.

The hydrogen atom diffusion mechanism on the DLC surface was discussed in analogy with the PCI case (Sect. 3.2).[31] First, we assumed that the surface diffusion of H (D) atoms on the DLC occurs only via the thermal hopping mechanism. Under the assumption of thermal hopping mechanism, the steady state ratio of H and D atoms is given by Eq. (6). Using the difference of activation barriers (1 meV) of thermal hopping of H and D atoms,[32] $n_D/n_H = 1.6$ is obtained for temperature 20 K. The recombination yield determined for the D atoms (30%) and the steady state ratio $n_D/n_H = 1.6$ leads to the conclusion that the recombination yield of H atoms at 20 K would not exceed 50%, contrary to the experimentally found nearly 100% recombination yield (See Ref. 34 for the details of derivation of the values). This inconsistency presumably originated from the assumption of the thermal hopping mechanism, and therefore we concluded that quantum mechanical tunneling plays an important role in the H atom diffusion on the DLC surface. The observation of an enhancement in H_2 recombination at elevated temperatures indicates that the tunneling probability is enhanced by thermal activation; i.e., the H atom diffusion among most of the DLC surface sites is considered to proceed through a thermally assisted tunneling mechanism. However, since some fractions of H and D atoms readily recombined (i.e., the absence of a large kinetic isotope effect), a contribution from thermal hopping diffusion mechanism cannot be excluded for some adsorbed sites.

6. Proton-hole transfer in ice

The electrochemical behavior of ice is one of the most important aspects in the science of ice and liquid water because of its fundamental importance and relevance to various fields of science, such as biochemistry and atmospheric chemistry.[71] Since the study by von Grotthuss at the beginning of the 1800s,[72] water ice has been widely accepted to carry a positive current by the transfer of excess protons via H_3O^+, similar to a "p-type" semiconductor. Although the proton transfer is still a matter of controversy at low temperatures and is therefore addressed both experimentally and theoretically,[73, 74] this phenomenon can be well described by the Grotthuss mechanism (see Fig. 9(a)).

In contrast, although "proton-hole transfer (PHT)" has been theoretically proposed as a possible mechanism for delivering negative charges in water ice (see Fig. 9(b)),[75] no clear evidence for the occurrence of this mechanism has been provided. The PHT, which is the relay of the proton abstraction of an OH^- ion from neighboring H_2O, was first considered as a "mirror image" concept of the Grotthuss mechanism a hundred years ago.[76] The PHT and the Grotthuss mechanisms were considered to be related straightforwardly. However, in liquid water, the mechanism of OH^- migration was found to differ from the PHT concept,[77] and in recent years, the migration of OH^- in liquid water was reported to be much less effective than proton transfer.[78] For ice, the negative current by the PHT has not been observed.[79] Consequently, the concept of the negative current conductivity by the PHT has remained to be confirmed both theoretically and experimentally for a hundred years. This is the reason why ice is still considered mainly as a "positive current conductor".

We recently first observed a negative constant current through ice upon UV photon exposure at temperatures below 50 K,[80] where proton transfer from the surface to the ice bulk making a positive current is significantly suppressed.[81] State-of-the-art

quantum chemical calculations indicate that the flow of negative current is caused by the PHT mechanism triggered by the UV-synthesis of OH on the ice surface.[80] ASW with 40 or 120 monolayers was deposited over a nickel-plated sapphire disk that was cooled by a He refrigerator. The current through the ice was measured at the nickel surfaces by a picoammeter. We observed a negative charge flow through the ice upon UV exposure in an ultrahigh vacuum chamber, as shown in Fig. 10. In the present experiment, the UV photons from a commercial deuterium lamp can photolyze H_2O into several channels, such as OH + H, O + H_2, O + 2H, and H_3O^+ + OH + (*D*-defect + e^- + vacancy) from $2H_2O$.[82] The first one, OH + H, is the dominant pathway in the energy region of photons from the lamp.[83] In addition, the UV photons create photoelectrons at the wall of metal surfaces within the chamber because the photons were not collimated toward the ice surface. It was considered that both the photoelectrons that landed on the ice surface and photofragments play a role in the appearance of the negative current. Among the fragments, lighter elements such as H and H_2 tend to carry the momentum and thus desorb at photodissociation. At the surface, the OH radicals would capture electrons attached from the gas phase to become OH^- because they have a higher electron affinity of ~1.8 eV than the other photofragments.[84][85] Therefore, the formation of OH^- ions on the surface would be followed by the negative charge flow.

To support this scenario, the instrument was modified so that the UV photon and electron irradiation could be separately controlled. By putting a housing with a glass capillary collimator on the UV source, the UV photons illuminate the ice surface only without creating undesired photoelectrons in the vacuum chamber. In addition, an electron gun was installed in front of the substrate surface. The constant negative current was observed only upon the operation of both the UV lamp and the electron gun, as shown

in Fig. 11. The transient negative current at the initial electron irradiation was previously reported to be a result of solvated electrons in the ice.[86] Further experiments were performed to understand how OH and electrons work for the negative current. The ice was first exposed only to UV photons for a given number of periods and subsequently exposed only to electrons. Because the OH radicals cannot move on the ice surface at low temperatures, roughly below 100 K, due to strong hydrogen bonding, the OH radicals can remain intact on the surface. Therefore, if OH^- formation at the surface triggers the negative conductivity, the current should appear even after the termination of UV operation. Fig. 12 shows the behaviors of currents through the ice when the ice was sequentially exposed to UV photons and electrons. When the ice was exposed only to UV, a positive current was observed. Subsequently, a negative current appeared immediately upon the application of electrons to the UV-irradiated ice, and it gradually decreased. The peak current seems to correlate with the duration of the UV irradiation; i.e., the peak current was approximately 5.5, 5, 4, and 2.5 nA after UV irradiations for 120, 60, 30, and 10 s, respectively. We suggest that these observations can be rationalized by the following processes. The positive current upon exposure to UV is presumably due to photoelectrons emitted from the nickel substrate to the ice-metal interface. The UV irradiation produces OH radicals on the surface, and the exposure to electrons produces OH^- ions. The OH^- ions are consumed by the flow of negative current, resulting in an exponential decrease in the current. The number of OH^- ions will be greater for a longer UV irradiation, which produced OH radicals, consistent with the correlation between the UV irradiation duration and the magnitude of the peak current. The results of a series of experiments shown in Figs. 10–12 strongly indicate that the negative current is caused by the PHT mechanism initiated by the formation of OH^- ions on the surface.

To confirm the occurrence of PHT, quantum chemical calculations were performed. The ONIOM (QM/MM) calculation[87] demonstrates that OH^- ions are not stable at the surfaces of both PCI and ASW, while the structure where OH^- is located within the bulk is energetically favorable. The calculated potential surfaces indicate that the potential minima of the OH^--ice system are connected without significant barriers (See Fig. 13). In fact, the atom-centered density matrix propagation (ADMP) trajectory calculation[88] using the wB97X-D/6-31G(d) level of theory[89] showed the delivery of negative charge through thePHT in the ice (Fig. 14). From the results of experiments and calculations, we conclude that the negative constant current through the ice results from PHT.

7. Nuclear spin conversion of H_2 on ASW

A hydrogen molecule has two nuclear spin isomers, the ortho and para states, for total nuclear spins of 1 and 0 with spin multiplicities of triplet and singlet, respectively. At thermal equilibrium, the ortho/para nuclear spin ratio (OPR) of H_2 is expressed by functions of the temperature, which is the so-called nuclear spin temperature. Because the ortho and para spin isomers have rotational states with odd and even quantum numbers, respectively, observing the population of the rotational states of those molecules gives the OPR, in other words, the nuclear spin temperature. Radiative transition between ortho and para states is forbidden. Furthermore, as ortho-to-para (OP) conversion in the gas phase by spin exchange reactions with proton and ionic species like H_3^+ occurs very slowly,[48] the OPR has often been used as a tool to investigate the physical and chemical condition of the birthplace of molecules. The OPR of H_2 strongly affects not only the chemistry, like deuterium fractionation, in the gas phase[90] but also the gas dynamics of

core formation[42] because the energy difference between the ortho (J = 1) and para (J = 0) states is significant (14.7 meV).

In recent years, laboratory experiments have shed light on the behaviors of the OPR of H_2 molecules on ice. It was found that the OPR of nascent H_2 produced by H-H recombination has a statistical limit of 3[30] and gradually decreases if H_2 stays on the ice surface.[91] The ortho-to-para (OP) conversion rate is accelerated when O_2 molecules coexist on the ice surface because of magnetic dipole interactions.[92] The combination of the Stark effect and Fermi contact was first proposed as the OP conversion mechanism on ASW.[91] These works did not cover the ice temperature dependence of OP conversion, which may provide information on conversion-rate-limiting processes.

We recently measured the temperature dependence of the OP conversion rate on ASW in the range of 9.2–16 K, where the H_2 molecules can stably remain on the surface without desorption.[49] The experimental procedure was similar to that described in Fig. 2. The gaseous H_2 molecules at the OPR of 3 were deposited for 2–4 s on ASW as a collimated molecular beam at each temperature. The coverages were estimated to be less than 0.1 by the H_2 beam fluence. The coverage at 16 K was approximately 30% of that at 10 K for the same fluence because of the smaller sticking coefficient. The use of a molecular beam can avoid the undesired collision of H_2 with the chamber walls and the cold head before landing on the ASW, which can alter the OPR of gaseous H_2 in advance. After leaving the H_2 molecules on the ASW for a given time period (waiting time) after terminating the H_2 deposition, the OPRs were measured by the PSD-REMPI method. The measured H_2 intensities in each of the ortho and para states as a function of the waiting time are shown in Fig. 15. The intensity of H_2 in the J = 1 (ortho) state became weaker and that of the J = 0 (para) state became stronger, while the sum of the J = 0 and 1 signals

remained approximately the same; thus, the OPR decreased from 3 over time. The OP conversion rates, τ^{-1}, were derived at each temperature of the ASW, as plotted in Fig. 16. The conversion rate steeply increases with the temperature. We first examined the influence of the adsorption site on the conversion rate. The depth of the adsorption potential on the ASW has a wide distribution unlike that on crystalline ice.[93, 94] At higher temperatures, because H_2 cannot stay at shallow potential sites, it tends to be trapped at deeper sites. At deeper sites, interaction between H_2 adsorbates and the surface would be stronger and thus may lead to a faster conversion as reported on other materials.[35, 95] We compared the conversion rate at 10 K for H_2 prepared in two different procedures: in one procedure, H_2 was deposited at 10 K, and in the other procedure, the temperature was lowered to 10 K immediately after H_2 deposition at 12 K. For the latter case, H_2 would stay at relatively deeper sites. The results were found to be equivalent for both cases. Therefore, we concluded that the conversion rate is governed by the temperature itself rather than the type of adsorption sites.

The OP conversion requires the energy dissipation process because the para state is energetically lower than the ortho state. Therefore, the role of phonons in the energy relaxation should be considered. The phonon process generally shows a temperature dependence and thus may be able to explain the steep temperature dependence. Among the phonon processes for spin-lattice relaxation, the obtained temperature dependence below 14 K is best fitted by the equation for the two-phonon Raman process, whose rate is proportional to the ca. 7th power of the temperature when the temperature is sufficiently lower than the Debye temperature of the solid.[96] Although the energy difference between the lowest ortho and para states is approximately 14.7 meV for isolated H_2, it should be lowered on the surface because of hindered rotation.[97] In any case, an inelastic neutron-

scattering experiment indicated that the acoustic phonon modes of vapor-deposited ASW at 50 K cover energies below approximately 23 meV with two very broad peaks centered at approximately 7 and 17 meV.[98] A phonon mode at ~6 meV was also observed in a surface-sensitive He-scattering experiment.[99] It is not clear why the behavior of the conversion rates above 14 K does not follow a power law. The rate could be limited purely by the spin conversion process. Very recently, it was claimed that the strong temperature dependence can be explained solely by the electromagnetic nature of the process.[100]

Acknowledgments

We would like to thank our colleagues, Professor A. Kouchi, Drs. H. Hidaka, Y. Oba, T. Hama, W. M. C. Sameera, and Y. Kimura for performing the series of works together. We also thank the technical staff at the ILTS for constructing and improving the parts of our instruments.

References

*watanabe@lowtem.hokudai.ac.jp

1) E. Herbst, J. Phys. Chem. A **109**, 4017 (2005).

2) E. A. Bergin and M. Tafalla, Annu. Rev. Astron. Astrophys. **45**, 339 (2007).

3) E. F. v. Dishoeck and G. A. Blake, Annu. Rev. Astron. Astrophys. **36**, 317 (1998).

4) W. M. Irvine, P. F. Goldsmith, and Å. Hjalmarson, in *Interstellar Processes*, edited by D. J. Hollenbach and H. A. Thronson (D Reidel Publishing, Dordrecht, 1987), pp. 560-609.

5) https://cdms.astro.uni-koeln.de/classic/molecules

6) E. L. Gibb, D. C. B. Whittet, A. C. A. Boogert, and A. G. G. M. Tielens, Astrophys. J. Suppl. Ser. **151**, 35 (2004).

7) A. C. A. Boogert, P. A. Gerakines, and D. C. B. Whittet, Annu. Rev. Astron. Astrophys. **53**, 541 (2015).

8) N. Watanabe and A. Kouchi, Prog. Surf. Sci. **83**, 439 (2008).

9) E. F. van Dishoeck, E. Herbst, and D. A. Neufeld, Chem. Rev. **113**, 9043 (2013).

10) S. B. Charnley, A. G. G. M. Tielens, and S. D. Rodgers, Astrophys. J. **482**, L203 (1997).

11) R. J. Gould and E. E. Salpeter, Astrophys. J. **138**, 393 (1963).

12) J. V. Keane, A. G. G. M. Tielens, A. C. A. Boogert, W. A. Schutte, and D. C. B. Whittet, Astron. Astrophys. **376**, 254 (2001).

13) Y. Oba, N. Miyauchi, H. Hidaka, T. Chigai, N. Watanabe, and A. Kouchi, Astrophys. J. **701**, 464 (2009).

14) N. Miyauchi, H. Hidaka, T. Chigai, A. Nagaoka, N. Watanabe, and A. Kouchi, Chem. Phys. Lett. **456**, 27 (2008).

15) S. Ioppolo, H. M. Cuppen, C. Romanzin, E. F. van Dishoeck, and H. Linnartz,

Astrophys. J. **686**, 1474 (2008).

16) N. Watanabe and A. Kouchi, Astrophys. J. **571**, L173 (2002).

17) K. Hiraoka, N. Ohashi, Y. Kihara, K. Yamamoto, T. Sato, and A. Yamashita, Chem. Phys. Lett. **229**, 408 (1994).

18) G. W. Fuchs, H. M. Cuppen, S. Ioppolo, C. Romanzin, S. E. Bisschop, S. Andersson, E. F. van Dishoeck, and H. Linnartz, Astron. Astrophys. **505**, 629 (2009).

19) H. Hidaka, M. Watanabe, A. Kouchi, and N. Watanabe, Astrophys. J. **702**, 291 (2009).

20) D. E. Woon, J. Chem. Phys. **105**, 9921 (1996).

21) David E. Woon, Astrophys. J. **569**, 541 (2002).

22) H. J. Werner, C. Bauer, P. Rosmus, H. M. Keller, M. Stumpf, and R. Schinke, J. Chem. Phys. **102**, 3593 (1995).

23) S. Andersson and M. Grüning, J. Phys. Chem. A **108**, 7621 (2004).

24) T. Hama and N. Watanabe, Chem. Rev. **113**, 8783 (2013).

25) G. Vidali, V. Pirronello, L. Li, J. Roser, G. Manicó, E. Congiu, H. Mehl, A. Lederhendler, H. B. Perets, J. R. Brucato, and O. Biham, J. Phys. Chem. A **111**, 12611 (2007).

26) R. G. Smith, K. Sellgren, and A. T. Tokunaga, Astrophys. J. **344**, 413 (1989).

27) H. B. Perets, O. Biham, G. Manicó, V. Pirronello, J. Roser, S. Swords, and G. Vidali, Astrophys. J. **627**, 850 (2005).

28) E. Matar, E. Congiu, F. Dulieu, A. Momeni, and J. L. Lemaire, Astron. Astrophys. **492**, L17 (2008).

29) A. Ikeda and K. Fukutani, in *Compendium of Surface and Interface Analysis* (Springer Singapore, Singapore, 2018), pp. 487-492.

30) N. Watanabe, Y. Kimura, A. Kouchi, T. Chigai, T. Hama, and V. Pirronello, Astrophys. J. **714**, L233 (2010).

31) K. Kuwahata, T. Hama, A. Kouchi, and N. Watanabe, Phys. Rev. Lett. **115**, 133201 (2015).

32) T. Hama, K. Kuwahata, N. Watanabe, A. Kouchi, Y. Kimura, T. Chigai, and V. Pirronello, Astrophys. J. **757** (2012).

33) Y. Kimura, M. Tsuge, V. Pirronello, A. Kouchi, and N. Watanabe, Astrophys. J. **858** (2018).

34) M. Tsuge, T. Hama, Y. Kimura, A. Kouchi, and N. Watanabe, Astrophys. J. **878**, 23 (2019).

35) K. Fukutani and T. Sugimoto, Prog. Surf. Sci. **88**, 279 (2013).

36) V. Wakelam, E. Bron, S. Cazaux, F. Dulieu, C. Gry, P. Guillard, E. Habart, L. Hornekær, S. Morisset, G. Nyman, V. Pirronello, S. D. Price, V. Valdivia, G. Vidali, and N. Watanabe, Mol. Astrophys. **9**, 1 (2017).

37) L. Pagani, E. Roueff, and P. Lesaffre, Astrophys. J. **739**, L35 (2011).

38) L. Pagani, P. Lesaffre, M. Jorfi, P. Honvault, T. González-Lezana, and A. Faure, Astron. Astrophys. **551**, A38 (2013).

39) E. Bron, F. Le Petit, and J. Le Bourlot, Astron. Astrophys. **588**, A27 (2016).

40) K. Furuya, Y. Aikawa, T. Hama, and N. Watanabe, Astrophys. J. **882**, 172 (2019).

41) D. C. Black and P. Bodenheimer, Astrophys. J. **199**, 619 (1975).

42) N. Vaytet, K. Tomida, and G. Chabrier, Astron. Astrophys. **563**, A85 (2014).

43) K. Takayanagi, K. Sakimoto, and K. Onda, Astrophys. J. **318**, L81 (1987).

44) D. R. Flower, G. Pineau Des Forêts, and C. M. Walmsley, Astron. Astrophys. **449**, 621 (2006).

45) D. Gerlich, J. Chem. Phys. **92**, 2377 (1990).

46) D. Gerlich, F. Windisch, P. Hlavenka, R. Plašil, and J. Glosik, Phil. Trans. Roy. Soc.

A: Math Phys. Eng. Sci. **364**, 3007 (2006).

47) J. Takahashi, Astrophys. J. **561**, 254 (2001).

48) D. R. Flower and G. D. Watt, Mon. Not. R. Astron. Soc. **209**, 25 (1984).

49) H. Ueta, N. Watanabe, T. Hama, and A. Kouchi, Phys. Rev. Lett. **116**, 253201 (2016).

50) V. Zumbach, J. Schäfer, J. Tobai, M. Ridder, T. Dreier, T. Schaich, J. Wolfrum, B. Ruf, F. Behrendt, O. Deutschman, and J. Warnatz, J. Chem. Phys. **107**, 5918 (1997).

51) A. Nagaoka, N. Watanabe, and A. Kouchi, J. Phys. Chem. A **111**, 3016 (2007).

52) A. E. Pomerantz, F. Ausfelder, R. N. Zare, and W. M. Huo, Can. J. Chem. **82**, 723 (2004).

53) V. Buch and Q. Zhang, Astrophys. J. **379**, 647 (1991).

54) K. Thürmer and N. C. Bartelt, Phys. Rev. B: Condens. Matter **77**, 195425 (2008).

55) R. P. Bell, *The Tunnel Effect in Chemistry*. (Chapman and Hall, New York, 1980).

56) T. Miyazaki, in *Atom Tunneling Phenomena in Physics, Chemistry and Biology*, edited by T. Miyazaki (Splinger, Berlin, 2003), pp. 59–90.

57) R. Smoluchowski, Astrophys. Space Sci. **65**, 29 (1979).

58) R. Smoluchowski, Astrophys. Space Sci. **75**, 353 (1981).

59) R. Smoluchowski, J. Phys. Chem. **87**, 4229 (1983).

60) K. M. Pontoppidan, H. J. Fraser, E. Dartois, W.-F. Thi, E. F. van Dishoeck, A. C. A. Boogert, L. d'Hendecourt, A. G. G. M. Tielens, and S. E. J. A. Bisschop, Astron. Astrophys. **408**, 981 (2003).

61) K. M. Pontoppidan, Astron. Astrophys. **453**, L47 (2006).

62) E. Habart, F. Boulanger, L. Verstraete, G. P. d. Forêts, E. Falgarone, and A. Abergel, Astron. Astrophys. **397**, 623 (2003).

63) E. Habart, F. Boulanger, L. Verstraete, C. M. Walmsley, and G. P. d. Forêts, Astron.

Astrophys. **414**, 531 (2004).

64) G. Vidali, Chem. Rev. **113**, 8762 (2013).

65) L. Hornekær, in *Laboratory Astrochemistry: From Molecules through Nanoparticles to Grains*, edited by S. Stephan, G. Thomas, M. Harald and J. Cornelia (Wiley-VCH, 2015), pp. 255–325.

66) D. C. B. Whittet, A. C. A. Boogert, P. A. Gerakines, W. Schutte, A. G. G. M. Tielens, T. de Graauw, T. Prusti, E. F. van Dishoeck, P. R. Wesselius, and C. M. Wright, Astrophys. J. **490**, 729 (1997).

67) C. W. Ong, X. A. Zhao, J. T. Cheung, S. K. Lam, Y. Liu, C. L. Choy, and P. W. Chan, Thin Solid Films **258**, 34 (1995).

68) J. Robertson, Materials Science and Engineering: R: Reports **37**, 129 (2002).

69) L. J. Allamandola, S. A. Sandford, A. G. Tielens, and T. M. Herbst, Science **260**, 64 (1993).

70) T. Henning and F. Salama, Science **282**, 2204 (1998).

71) T. Miyake and M. Rolandi, J. Phys.: Condens. Matter **28**, 023001 (2015).

72) S. Biochimica et Biophysica ActaCukierman, Biochim. Biophys. Acta **1757**, 876 (2006).

73) J. P. Devlin, Phys. Chem. Chem. Phys. **13**, 19707 (2011).

74) A. I. Kolesnikov, G. Ehlers, E. Mamontov, and A. Podlesnyak, Phys. Rev. B **98**, 064301 (2018).

75) D. Marx, ChemPhysChem **7**, 1848 (2006).

76) E. Hückel, Z. Elektrochem. **34**, 546 (1928).

77) M. E. Tuckerman, D. Marx, and M. Parrinello, Nature **417**, 925 (2002).

78) M. Chen, L. Zheng, B. Santra, H.-Y. Ko, R. A. DiStasio Jr, M. L. Klein, R. Car, and

X. Wu, Nat. Chem. **10**, 413 (2018).

79) D. H. Lee, C. H. Choi, T. H. Choi, B. J. Sung, and H. Kang, J. Phys. Chem. Lett. **5**, 2568 (2014).

80) N. Watanabe, W. M. C. Sameera, H. Hidaka, A. Miyazaki, and A. Kouchi, Chem. Phys. Lett. **737**, 136820 (2019).

81) J. P. Cowin, A. A. Tsekouras, M. J. Iedema, K. Wu, and G. B. Ellison, Nature **398**, 405 (1999).

82) V. F. Petrenko and N. N. Khusnatdinov, J. Chem. Phys. **100**, 9096 (1994).

83) O. Dutuit, A. Tabche - Fouhaile, I. Nenner, H. Frohlich, and P. M. Guyon, J. Chem. Phys. **83**, 584 (1985).

84) NIST Computational Chemistry Comparison and Benchmark DataBase, https://cccbdb.nistgov/elecaff1.asp

85) NIST Chemistry Webbook, https://webbook.nist.gov/chemistry/

86) R. Sagi, M. Akerman, S. Ramakrishnan, and M. Asscher, J. Phys. Chem. C **122**, 9985 (2018).

87) L. W. Chung, W. M. C. Sameera, R. Ramozzi, A. J. Page, M. Hatanaka, G. P. Petrova, T. V. Harris, X. Li, Z. Ke, F. Liu, H.-B. Li, L. Ding, and K. Morokuma, Chem. Rev. **115**, 5678 (2015).

88) S. S. Iyengar, H. B. Schlegel, J. M. Millam, G. A. Voth, G. E. Scuseria, and M. J. Frisch, J. Chem. Phys. **115**, 10291 (2001).

89) J.-D. Chai and M. Head-Gordon, Phys. Chem. Chem. Phys. **10**, 6615 (2008).

90) L. Majumdar, P. Gratier, M. Ruaud, V. Wakelam, C. Vastel, O. Sipilä, F. Hersant, A. Dutrey, and S. Guilloteau, Mon. Not. R. Astron. Soc. **466**, 4470 (2016).

91) T. Sugimoto and K. Fukutani, Nat. Phys. **7**, 307 (2011).

92) M. Chehrouri, J. H. Fillion, H. Chaabouni, H. Mokrane, E. Congiu, F. Dulieu, E. Matar, X. Michaut, and J. L. Lemaire, Phys. Chem. Chem. Phys. **13**, 2172 (2011).

93) L. Hornekær, A. Baurichter, V. V. Petrunin, A. C. Luntz, B. D. Kay, and A. Al-Halabi, J. Chem. Phys. **122**, 124701 (2005).

94) L. Amiaud, J. H. Fillion, S. Baouche, F. Dulieu, A. Momeni, and J. L. Lemaire, J. Chem. Phys. **124**, 94702 (2006).

95) T. Kosone, A. Hori, E. Nishibori, Y. Kubota, A. Mishima, M. Ohba, H. Tanaka, K. Kato, J. Kim, J. A. Real, S. Kitagawa, and M. Takata, R. Soc. Open Sci. **2**, 150006 (2015).

96) J. Van Kranendonk, Physica **20**, 781 (1954).

97) Y. Kunisada, H. Nakanishi, Di, Ntilde, W. A. O, and H. Kasai, J. Vac. Soc. Jpn. **55**, 115 (2012).

98) O. Yamamuro, Y. Madokoro, H. Yamasaki, T. Matsuo, I. Tsukushi, and K. Takeda, J. Chem. Phys. **115**, 9808 (2001).

99) A. Glebov, A. P. Graham, A. Menzel, J. P. Toennies, and P. Senet, J. Chem. Phys. **112**, 11011 (2000).

100) E. Ilisca, Chem. Phys. Lett. **713**, 289 (2018).

Figure captions

Fig. 1. Schematic illustration of the timing chart for the typical PSD-REMPI measurement for detecting H atoms on the ice surface. H atoms were continuously deposited on the ASW surface with a flux on the order of 10^{12} cm^{-2} s^{-1}. The H atoms on the surface was desorbed with the PSD laser (532 nm, 10 ns pulse width, 80 μJ $pulse^{-1}$) and, after a certain delay, selectively ionized by the REMPI laser. The H^+ thus produced was detected with a linear time-of-flight (TOF) mass spectrometer.

Fig. 2. (a) The PSD-REMPI spectra via the $2s \leftarrow 1s$ transition of H atoms photodesorbed from the ASW surface after depositions of 1, 2, 3.8, and 5.6 s for the bottom to top spectra. (b) Increase of H atoms photodesorbed from ASW during the deposition of H atoms at 8 K, corresponding to an increase in the H-atom coverage.

Fig. 3. Timing chart for the experiment to measure the H-atom attenuation on the ice surface. A given amount of H atoms was deposited on the surface of the ASW. After the waiting time (t), the atoms were detected with the PSD-REMPI method. Because the surface number density of the H atoms is expected to decrease due to the H-H recombination reaction and/or monoatomic desorption, the H signal intensity will be attenuated with the increasing waiting time.

Fig. 4. Time evolution of the total H_2 ($J = 0$ and 1) signal intensities photodesorbed from (a) the aluminum (Al) substrate and (b) amorphous solid water (ASW) at 8 K as a

function of the H_2 deposition time (filled circles) and H atom deposition (open circles). The delay time between the PSD and REMPI lasers was set to give the maximal PSD-REMPI intensity.

Fig. 5. Attenuation of the PSD-REMPI intensities of photodesorbed H atoms (circles) and D atoms (squares). The filled symbols represent the results on the ASW surface, and the open symbols represent those on the PCI surface. The solid lines are fits assuming E_{diff} = 22 meV and 23 meV at 8 K for H and D atoms, respectively, with Eq. (2). The dotted line is the attenuation curve simulated by assuming E_{diff} = 30 meV at 8 K.

Fig. 6. The ratio of the D and H atom intensities obtained by the PSD-REMPI method during the continuous deposition on PCI (pink) and ASW (blue) surfaces as a function of the atom flux. The right vertical axis represents the ratio of the surface diffusion rates calculated from Eq. (6). The shaded area represents the thermal-diffusion dominated region derived from Eqs. (3) and (6).

Fig. 7. Attenuation of the PSD-REMPI intensities of H atoms (filled symbols) photodesorbed from the pure solid CO at 8 K (square), 12 K (circle), and 16 K (triangle) after the accumulation of the H atoms. The solid curves are the best-fit curves of the attenuation of H atoms by recombination (Eq. (2)). The result of the measurements of D atoms at 8 K is shown by open squares; the intensities were normalized to the H atom intensity with the waiting time of 200 s.

Fig. 8. Time variation of the PSD-REMPI signals measured during (left column) H_2 or H atom deposition and (right column) D_2 or D atom deposition. The sample temperature was 8 and 20 K for the top and bottom panels, respectively. The signals following molecular deposition are shown in black lines, and those following atomic deposition are in red lines. The sum of the H_2 ($J = 0$ and 1) signals is presented.

Fig. 9. Schematic drawing of the Grotthuss and proton-hole transfer (PHT) mechanisms for a water ice sample in a vacuum. Movements of protons or electrons are indicated with arrows. In (a), the process is initiated by a hydronium ion, H_3O^+, at the ice-vacuum interface. The proton in this hydronium ion is transferred by proton hop processes. As a result, a positive current from the ice-vacuum interface to the metal substrate is observed. In (b), the process is initiated with the production of a hydroxyl ion, OH^-, at the ice-vacuum interface. The hydroxyl ion serves as a proton hole and is transferred by the proton transfer, resulting in a negative current.

Fig. 10. (a) Schematic drawing of the UV irradiation experiment. A water ice (ASW) sample with 40 or 120 monolayers was deposited over a nickel-plated sapphire substrate that was cooled by a closed-cycle He refrigerator. The ASW sample was irradiated with UV light (flux = 2.5×10^{13} cm^{-2} s^{-1}) provided from a deuterium lamp. The current through the ASW ice was measured at the nickel surface by a picoammeter. (b) The variation of the current through the ice; a negative current was observed only during the UV irradiation.

Fig. 11. (a) Schematic drawing of the UV and electron irradiation experiment. The sample

was prepared similarly to the one shown in Fig. 10. The UV light from a deuterium lamp was introduced through a capillary plate so that the UV photons only illuminate the ice surface without creating unwanted photoelectrons. Electrons with a 30 eV kinetic energy were provided from an electron gun installed in front of the sample surface. (b) The variation of the current through the ice observed in this type of experiment.

Fig. 12. The behaviors of the currents through an ASW sample when the sample was sequentially exposed to UV photons and electrons. The duration of the UV irradiation is indicated, and that of the electron exposure was ~200 s.

Fig. 13. The OH^- migration paths through the PHT mechanism in (a) crystalline water ice I_h and (b) amorphous ice calculated by the ONIOM (QM/MM) method. A portion of calculated system is depicted on the left side, where molecules calculated with the QM method are shown in dark color and those calculated with the MM method in thin color. Curved arrows indicate the motion of protons at each step. The obtained energy diagrams are shown on the right side. The energy at LM1 is used as the reference. SP, LM, and TS stand for starting point, local minimum, and transition state, respectively.

Fig. 14. (a) Schematic diagram showing the OH^- migration path. The ADMP trajectory for the initial proton abstraction process on crystalline hexagonal ice (I_h) calculated using the wB97X-D/6-31G(d) level of theory. (b) Progress of O(1)-H(A) and O(5)-H(A) distances. (c) Progress of O(2)-H(B) and O(1)-H(B)

distances. (d) Progress of O(3)-H(C) and O(2)-H(C) distances. (e) Progress of O(4)-H(D) and O(3)-H(D) distances.

Fig. 15. The PSD-REMPI intensities of H_2 photodesorbed from ASW at 16 K for $J = 0$ (bottom) and $J = 1$ (top) at different residence times (from top to bottom traces: 10, 300, and 600 s). The H_2 (OPR = 3) was deposited on the ASW at 16 K.

Fig. 16. Temperature dependence of the OP conversion rate for H_2 on ASW. The broken line represents the result of fitting the data with a power law of the form AT^n. The best fit for the temperature range 9.2–12 K was obtained for the values $A = 3.2 \times 10^{-11}$ s^{-1} and $n = 7.1 \pm 3.6$.

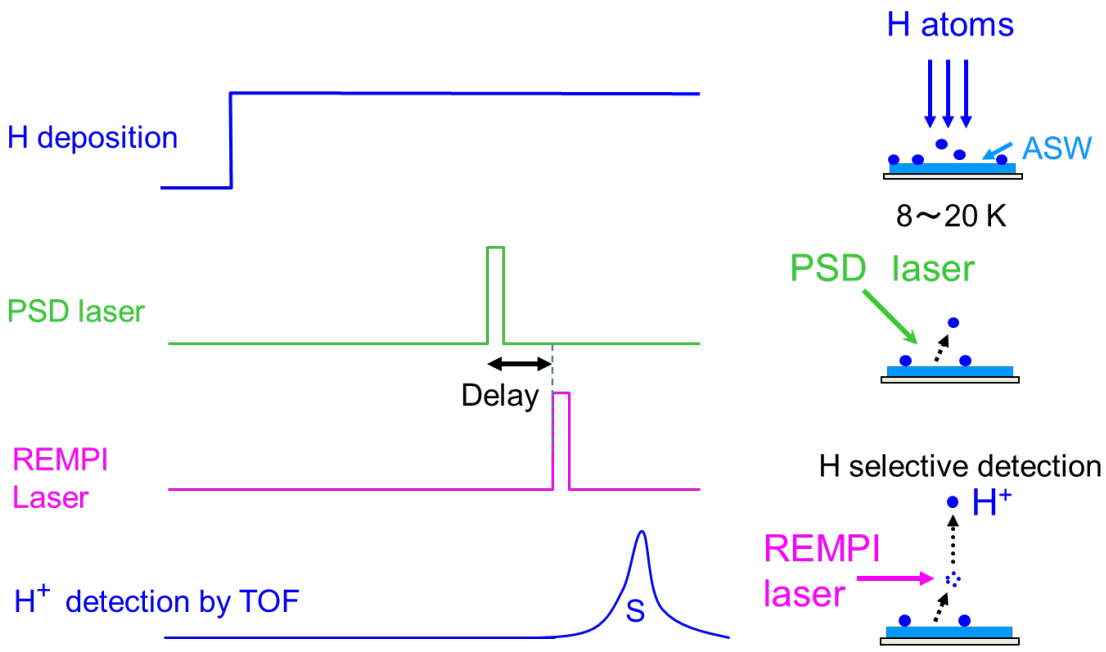

Fig. 1. Watanabe and Tsuge

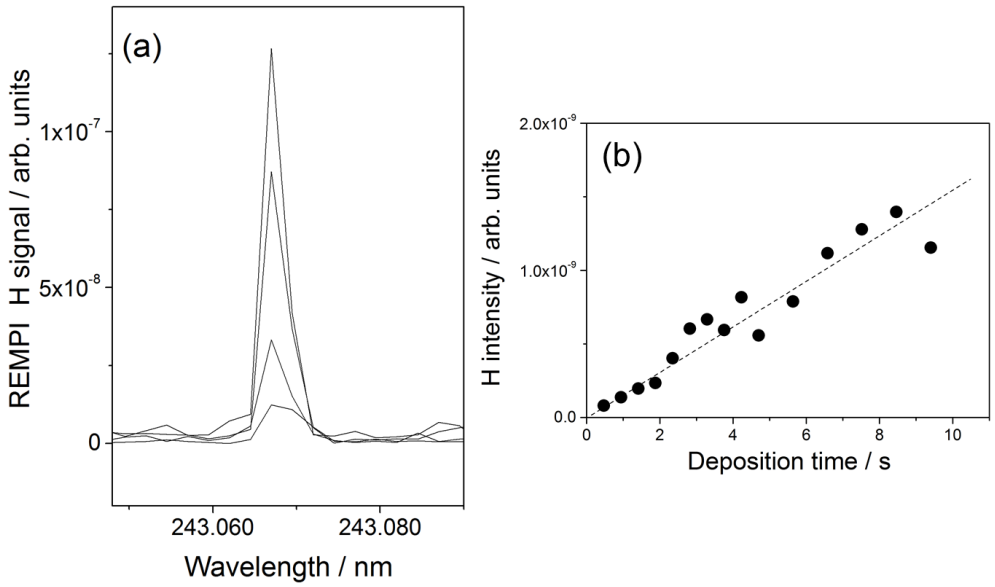

Fig. 2. Watanabe and Tsuge

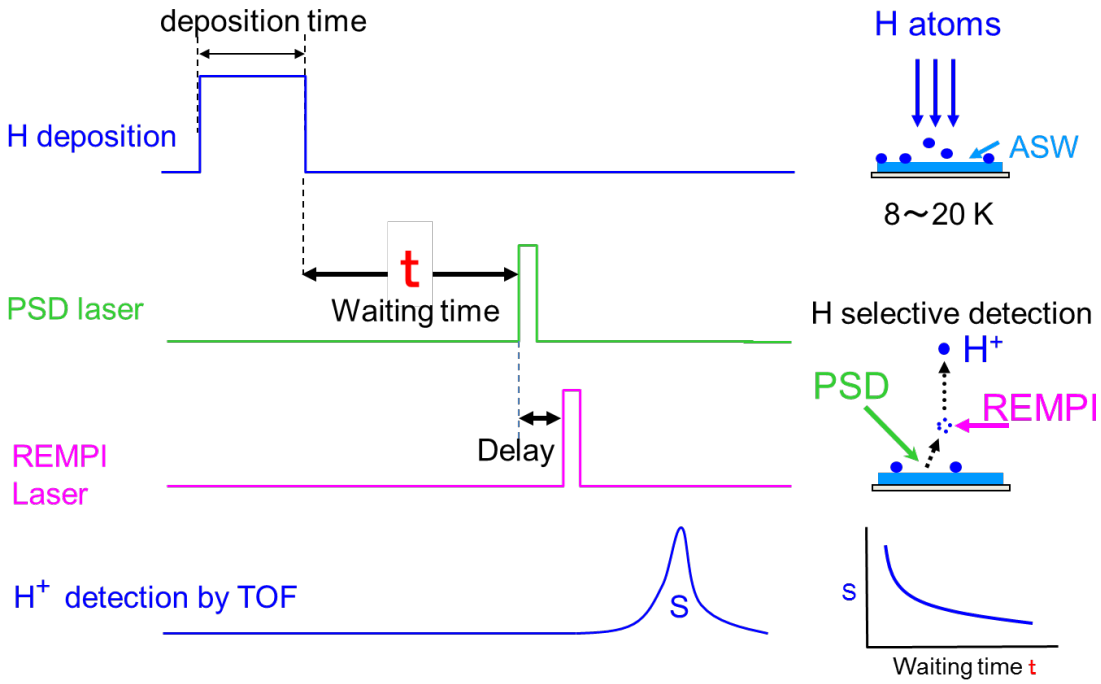

Fig. 3. Watanabe and Tsuge

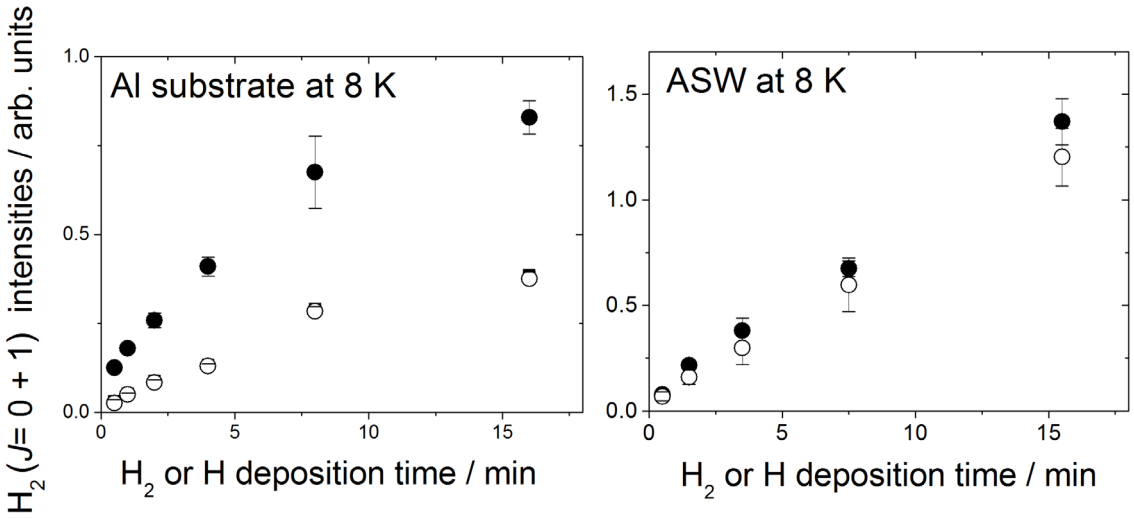

Fig. 4. Watanabe and Tsuge

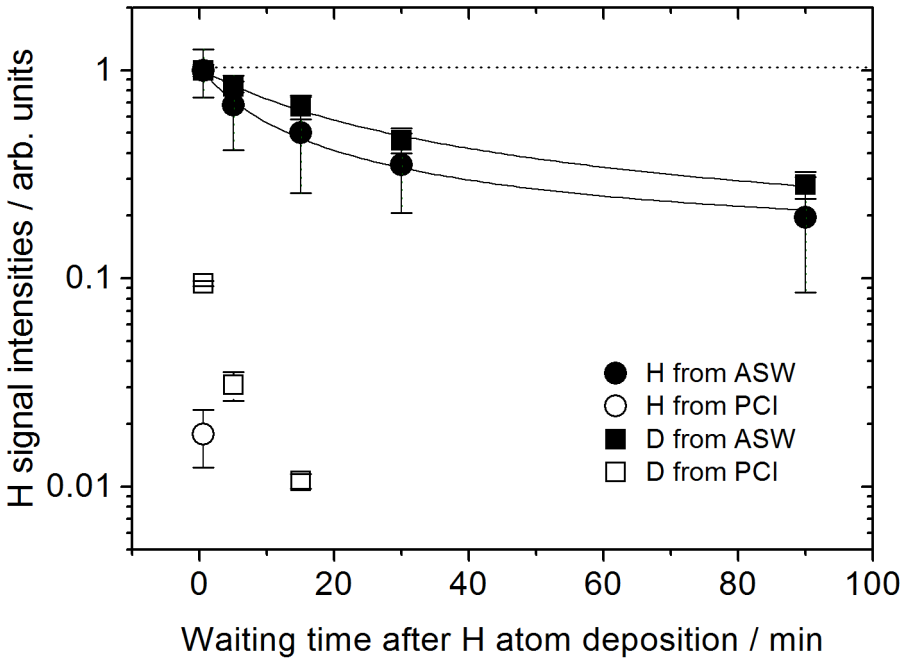

Fig. 5. Watanabe and Tsuge

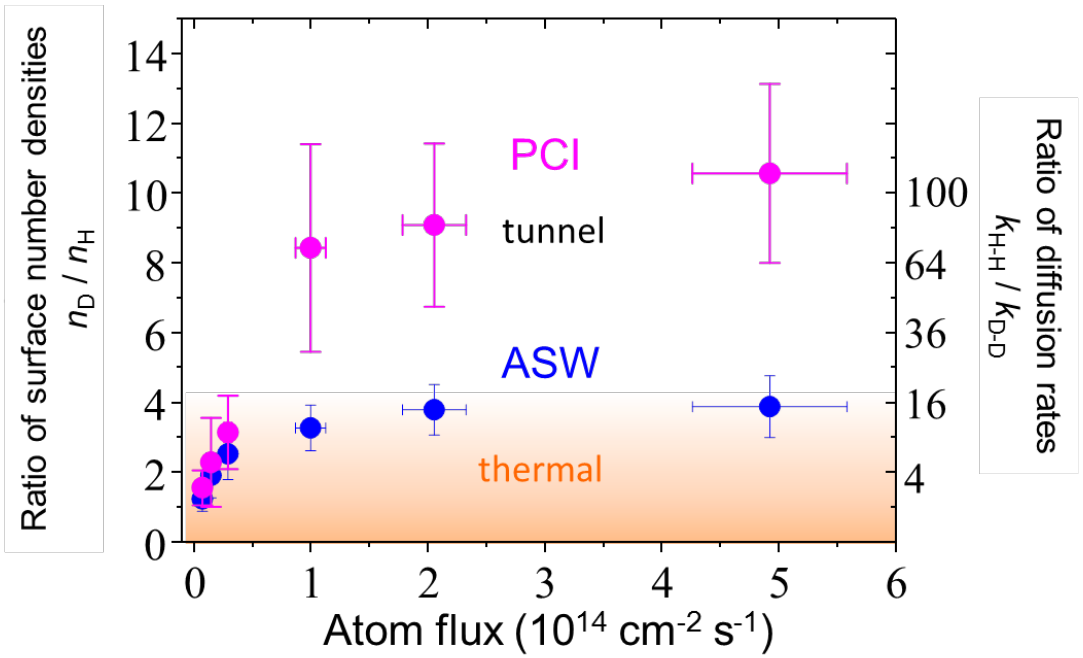

Fig. 6. Watanabe and Tsuge

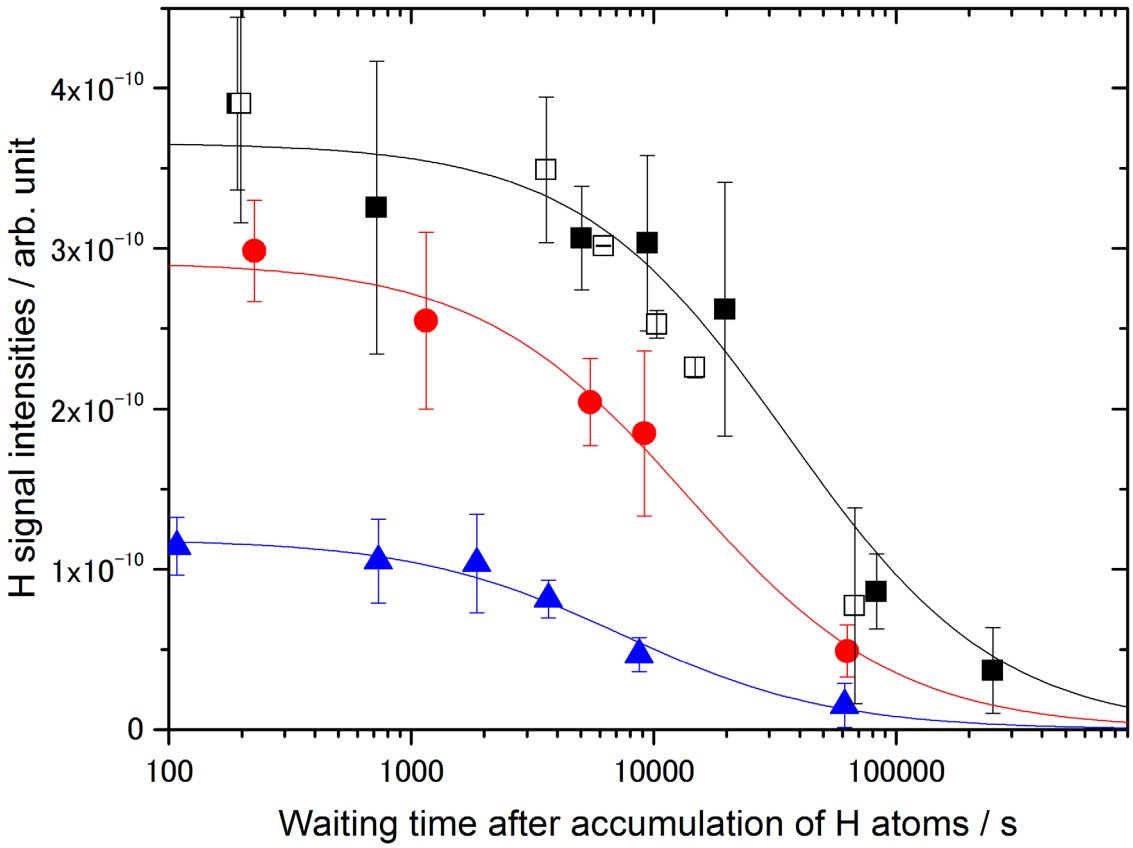

Fig. 7. Watanabe and Tsuge

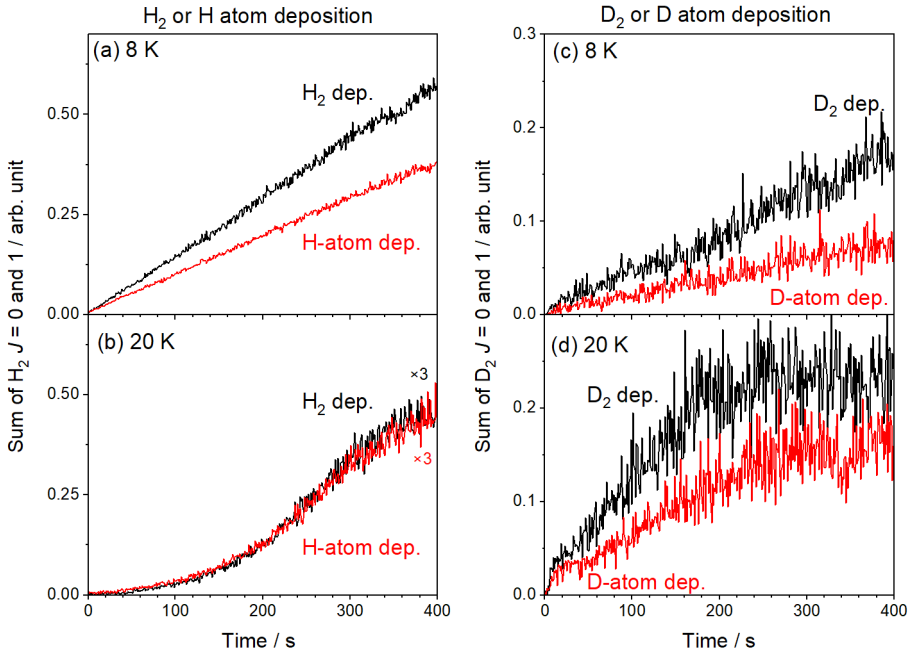

Fig. 8. Watanabe and Tsuge

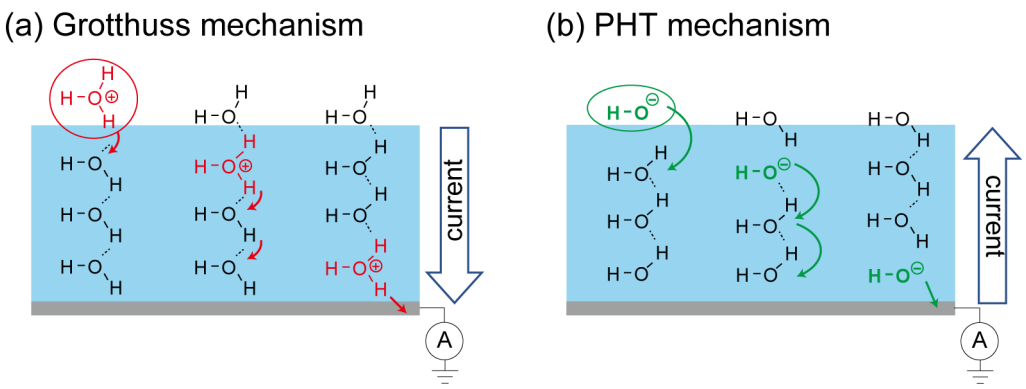

Fig. 9. Watanabe and Tsuge

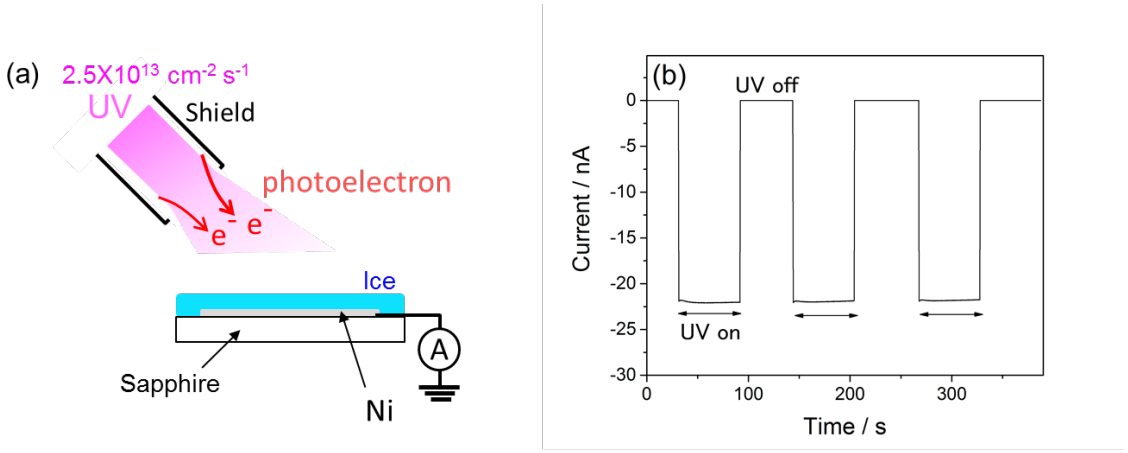

Fig. 10. Watanabe and Tsuge

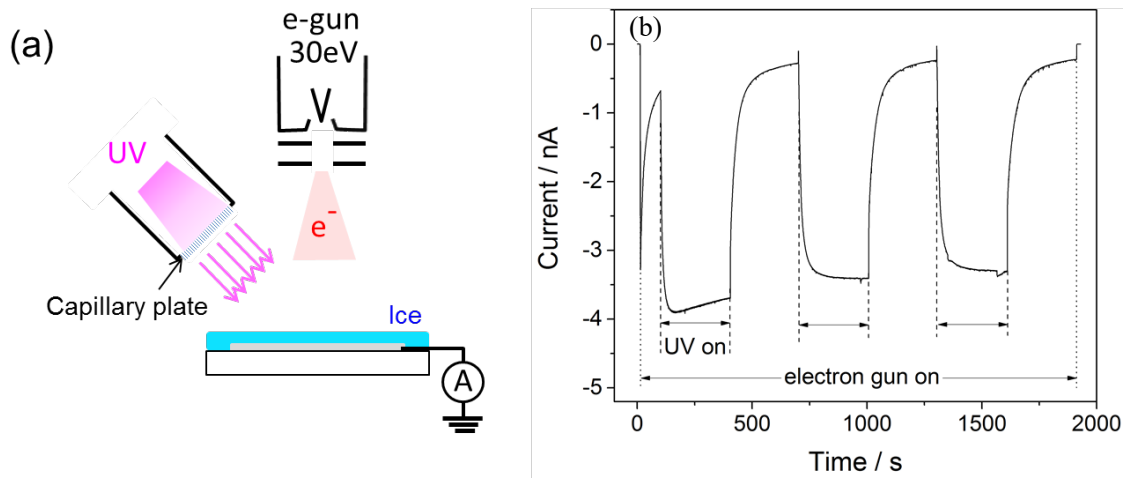

Fig. 11. Watanabe and Tsuge

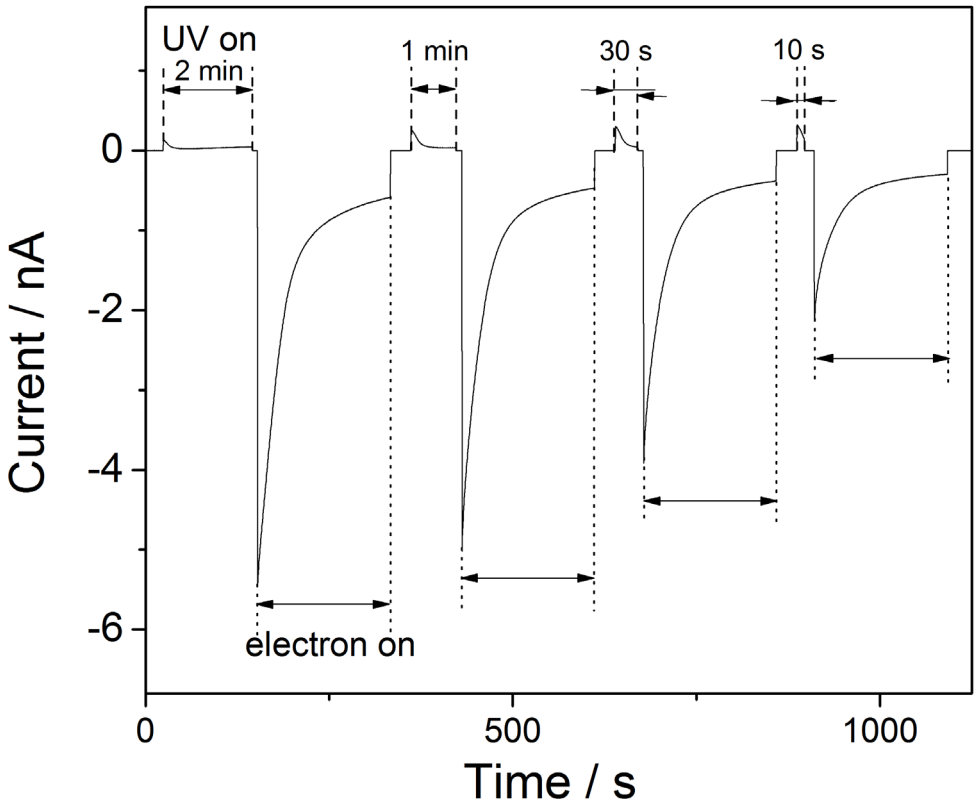

Fig. 12. Watanabe and Tsuge

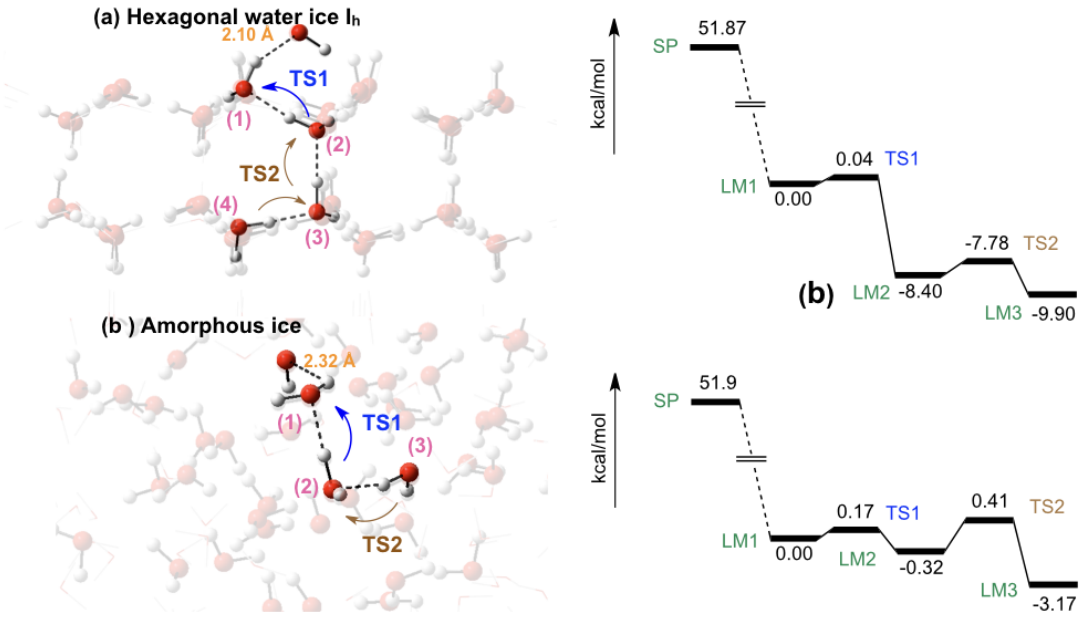

Fig. 13. Watanabe and Tsuge

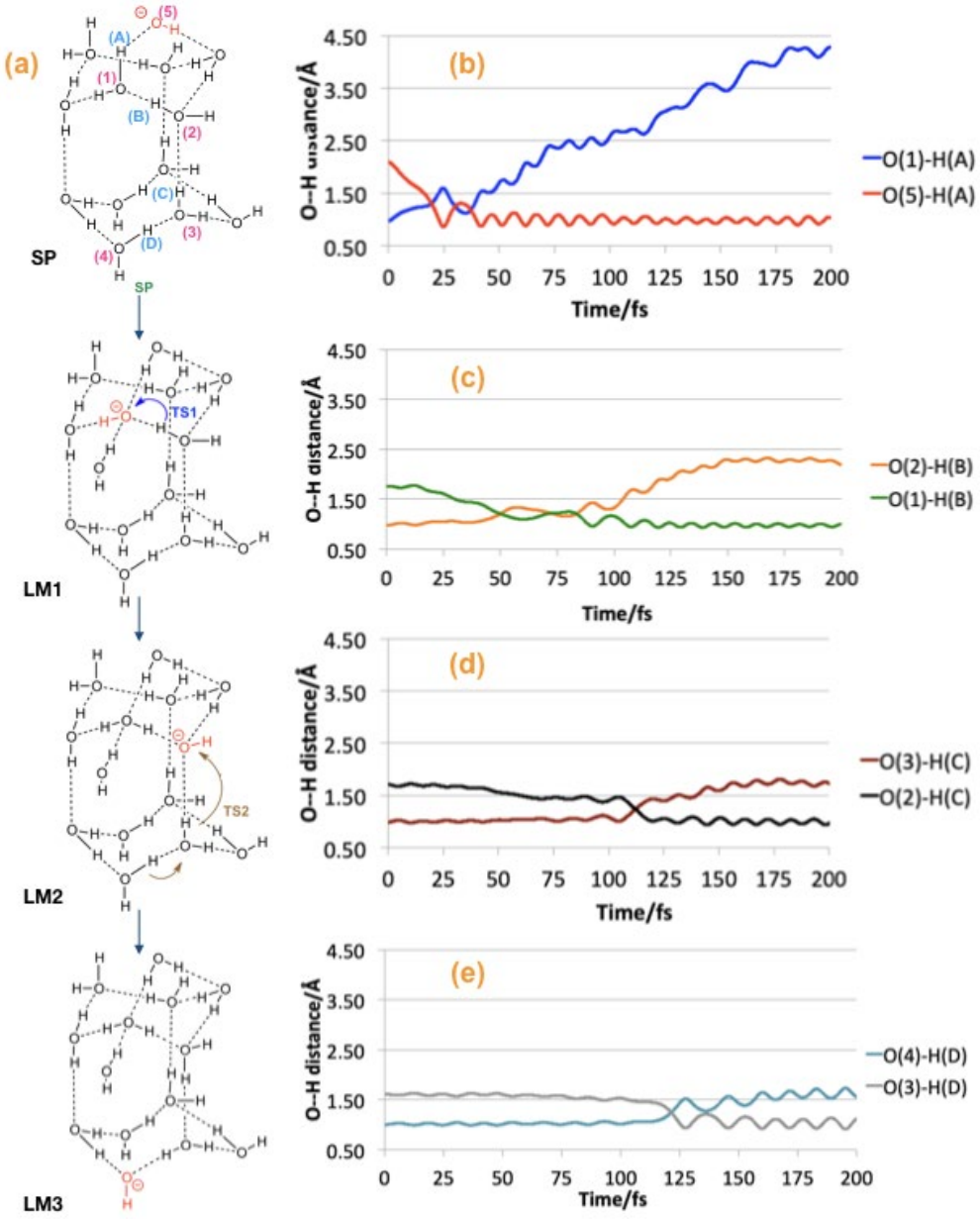

Fig. 14. Watanabe & Tsuge

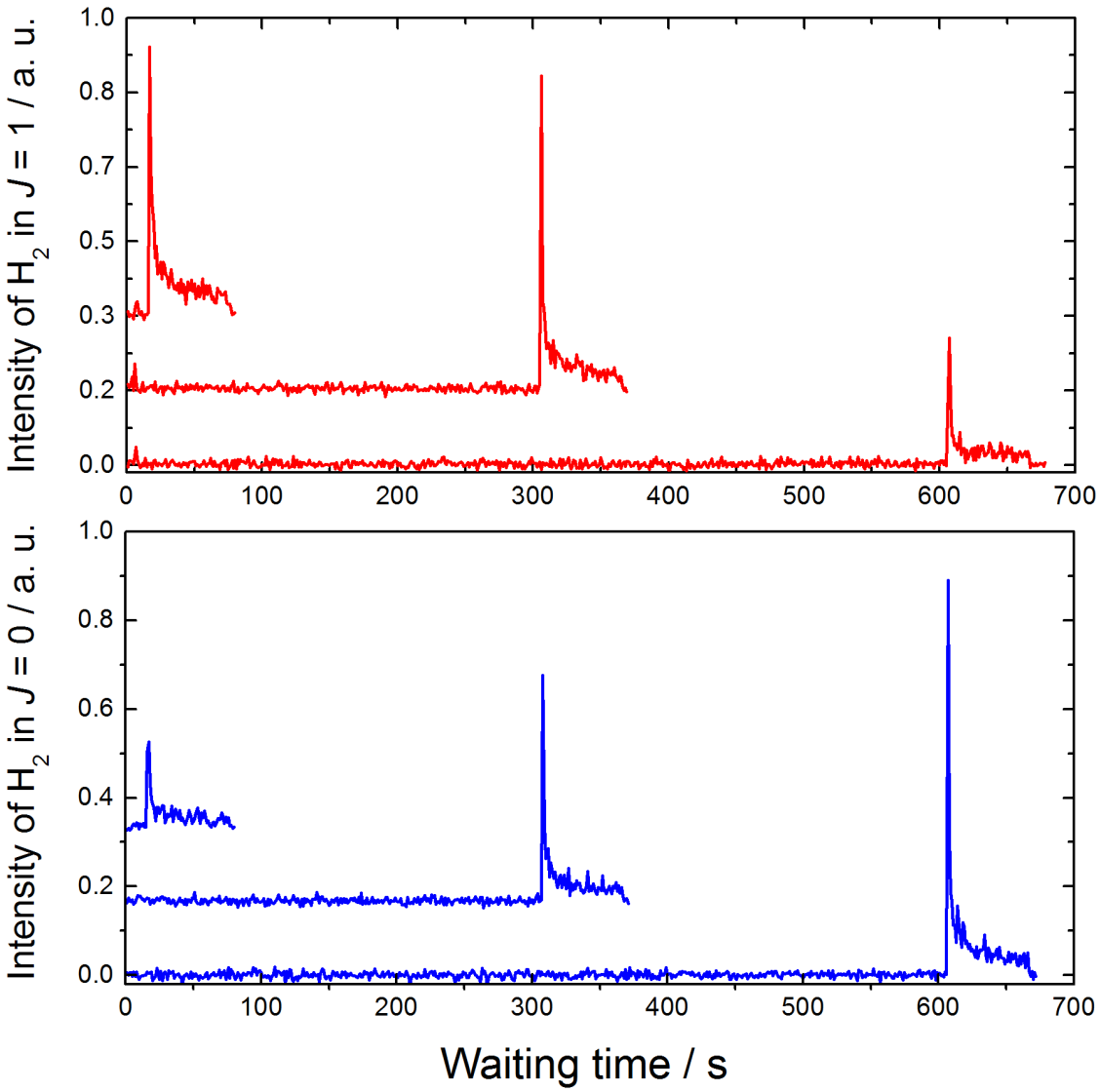

Fig. 15. Watanabe and Tsuge

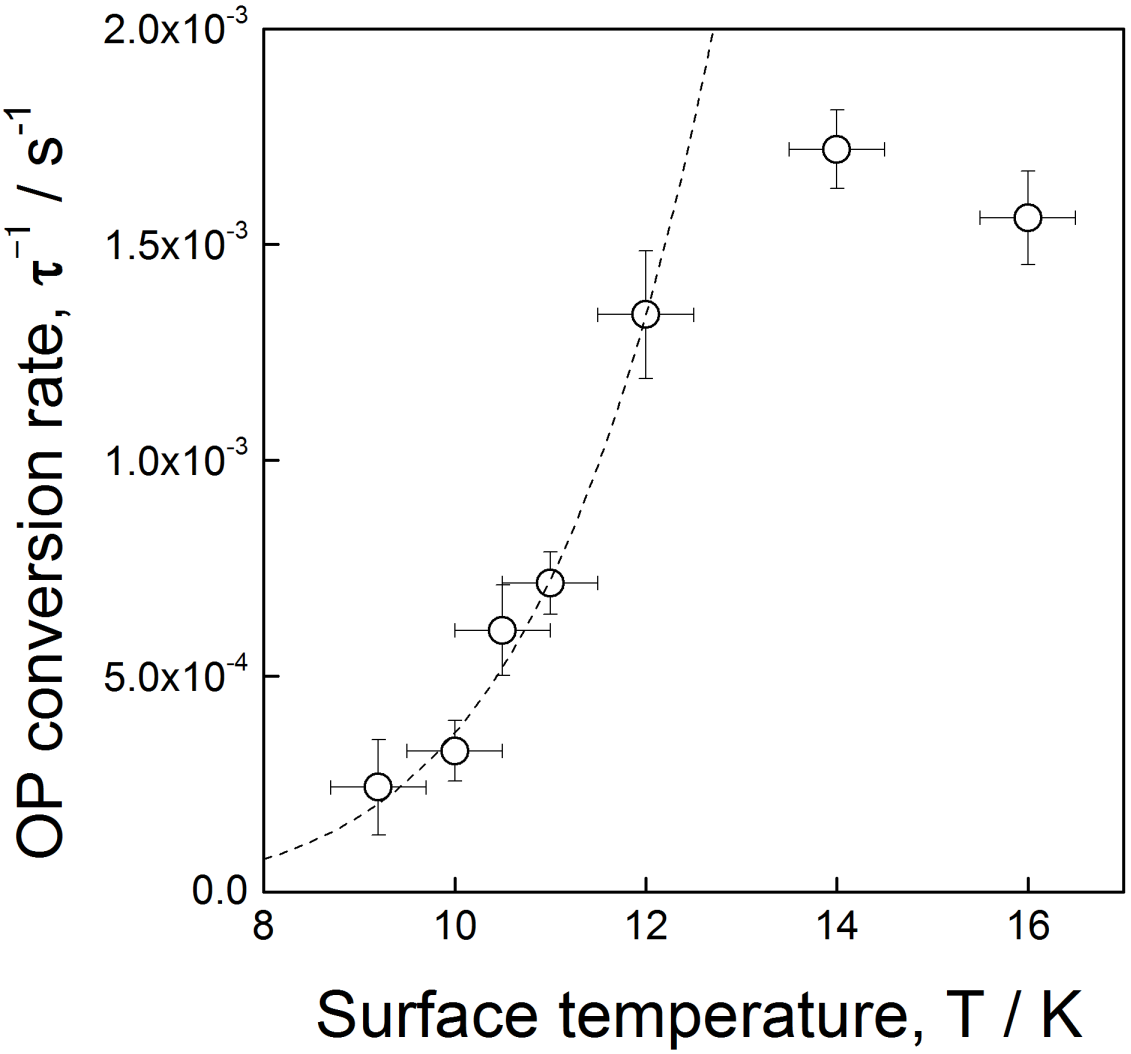

Fig. 16. Watanabe and Tsuge